International Journal of Mining and Geo-Engineering

IJMGE

IJMGE 54-2 (2020) 153-160

DOI: 10.22059/ijmge.2019.275091.594780

Geostatistical-based geophysical model of electrical resistivity and chargeability data applied to image copper mineralization in the Ghalandar deposit, Iran

Siavash Salarian [a], Omid Asghari [a,*], Maysam Abedi [b], Saeed Kazem Alilou [c]

[a] *Simulation and Data Processing Lab, School of Mining Engineering, College of Engineering, University of Tehran, Tehran, Iran*

[b] *GeoExploration Targeting Lab (GET-Lab), School of Mining Engineering, College of Engineering, University of Tehran, Tehran, Iran*

[c] *School of Mining Engineering, College of Engineering, University of Tehran, Tehran, Iran*

Article History:

Received: 30 January 2019,

Revised: 24 May 2019,

Accepted: 26 May 2019.

ABSTRACT

This research aims to construct 3D geophysical models of electrical resistivity and induced polarization by interpolating 2D inverted physical models through the geostatistical approach. The applicability of the method was examined for the Ghalandar porphyry-skarn copper deposit in the Agh-Daragh region, northwest of Iran. The 3D geophysical properties and block models of Cu grades were prepared by implementing the kriging interpolation method, whereby the recovered electrical models were closely linked to the Cu-sulfide mineralization. In order to evaluate the efficiency of the applied technique, the variogram models were validated using a cross-validation analysis of the kriging operation, proving the accuracy of data interpolation for each model. For the sake of meaningful correlation between geophysical models and Cu grades, the mineralization zones were extracted and subsequently propagated in the 3D space according to the generated physical properties. Meanwhile, the evaluation matrix was utilized to assess the performance of acquired results, where it confirmed that simultaneous consideration of physical models could much better determine the location of the copper mineralization. Also, the Swath plot was used as a second validation way to compare the anomalous zones.

Keywords : *Chargeability, Copper Mineralization, Cross-Validation, Electrical Resistivity, Kriging*

1. Introduction

Sulfide ore deposits are the main source of copper in the world, to which various geophysical surveys are applied to provide valuable information on the exploration of such sulfide-related targets [1]. Among the geophysical tools used in targeting these sources, the electrical properties of constituent materials with sharp contrasts are the most popular ones [2]. Constructing a 3D model of the blind target is the most important goal in geophysical explorations, while the model recovered from geophysical data inversion gives insights into the approximate geometry of the target. Electrical Resistivity Tomography (ERT), through a time-domain direct current survey, generates valuable information in close association with rock types and alterations [3]. Electrical resistivity (Rs) and induced polarization (IP) properties are usually derived from the ERT survey, which can delineate the location of sulfide-related copper mineralization. The integration of IP and Rs models has been successfully applied to detecting such sources [4]. The exploration of sulfides via Rs and IP methods is highly efficient due to electrical contrasts, and hence, the deposits with sulfides and oxides are generally identified by low resistivity and high chargeability values [5-10]. Laboratory measurements have shown that most of the sulfides represent IP effects that are larger than silicates and iron oxides [2]. However, IP responses are influenced by complex physical conditions [11-12].

Minerals and rocks associated with hydrothermal alterations in sulfide-bearing ore mineralization systems are recognized by distinct anomalous electrical properties. Also, geophysical methods, which are capable of localizing and modeling such electrical properties, are mainstays in the mineral exploration targeting of sulfide-related copper deposits. Indeed, electrical properties reflect the type and intensity of hydrothermal alterations related to these sources. The hydrothermal products that generate significant geophysical signatures are including pyrite, chalcopyrite, chalcocite, biotite, and sericite [13-14].

The dispersed nature of copper mineralization in sulfide-related systems is particularly suitable for IP surveys [15], initially developed for the exploration of porphyry copper deposits [16]. As a complex phenomenon, the IP anomalies reflect the ability of a rock to act as an electrical capacitor, where such characteristic is manifested in sulfide-bearing targets. Generally, the strongest IP anomalies are in association with quartz-sericite-pyrite alterations, mostly occurring in the sulfide-bearing systems [13-14]. The potassic alteration zone in the core is depleted of sulfide contents. The surrounding sericitic/phyllic alteration zone, however, has a higher sulfide content (e.g., pyrite), which itself is surrounded by the distal propylitic alteration zone with lower amounts of pyrite. In other words, the sericitic/phyllic alteration zone possesses the strongest IP anomalies in such mineralization systems [14].

Geostatistics, as a robust methodology in geospatial data interpolation, can add restrictions on spatial correlation, data conditioning, and incorporation of different scales [17]. The integration of geostatistics with geophysics has been widely used to tackling problems that arise from geophysical data modeling [4, 17-21]. Ramazi and Jalali (2014) investigated the application of geophysical inversion

* Corresponding author. Tel.: +989122183503, *E-mail address:* o.asghari@ut.ac.ir (O. Asghari).

and geostatistical simulation to constructing electrical models on the basis of interpolating 3D physical properties from the 2D inverted ERT data. They used the IP and Rs models for qualitative and quantitative evaluations of a copper deposit, on which the Sequential Gaussian Simulation (SGS) was utilized to map the spatial distribution of physical models. Their results helped them optimize the location of exploratory boreholes [21]. Asghari et al. (2016) studied multivariate geostatistics based on a model of geo-electrical properties for copper grade estimation. They aimed to reduce the variance of estimation and related uncertainty. This method can be useful when a sporadic pattern of boreholes exists. In this study, the sulfide factor was incorporated as a secondary correlated variable to estimate Cu grade distribution. The results showed that the use of a secondary variable causes better results in comparison with ordinary kriging [22].

This work is focused on the Ghalandar sulfide-bearing copper deposit in the Eastern Azerbaijan province. The ultimate motive of research was to localize and extract Cu-bearing zones through a geophysical survey of the ERT, where those promising zones would be suggested for drilling to acquire information about the geometry of blind targets. The geostatistical tools were employed to the 2D inverted ERT data in order to construct the 3D models of electrical resistivity and induced polarization. Those recovered models were in close association with the Cu-bearing zones when simultaneous consideration of both of the models was taken into account. The validity of the implemented method was also confirmed by an evaluation matrix between Cu mineralized zones and those from geophysical models. The swath plots were also carried out to investigate the trends of three variables (i.e., IP, Rs, Cu) in the direction of three main axes.

The remaining sections of this work are prepared as follows. The second section discusses the geological setting of the Ghalandar deposit in the Agh-Daragh area, NW of Iran. Geophysical data modeling is explained in the third section, where the ERT data have been inverted along 2D sections. Then, in section four, the geostatistical approach is utilized to construct 3D physical models of electrical resistivity and induce polarization. At the end of this section, the validity of the applied methodology is discussed in detail. Finally, the last section summarizes the main outcomes of this research in constructing a 3D geometry of the copper mineralization.

2. Geological Setting of the Ghalandar Porphyry-Skarn Deposit

The Northward Neo-Tethys subduction started in the Mesozoic, which led to the generation of the Iranian plateau [23-24]. Igneous activities in this subduction zone created a thick belt of mostly Cenozoic volcanic and plutonic units that is known as the Urmia-Dokhtar Magmatic Arc (UDMA), which is shown in Fig. 1. This belt has generated a distinct, linear intrusive-extrusive complex, located between and parallel to the Sanandaj-Sirjan Metamorphic Zone (SSZ) and the central Iran microcontinent [25]. The Agh-Daragh mineral prospect, which is the case study in this work, is located within the UDMA zone (Fig. 2). The UDMA (also known as the Sahand-Bazman or Tabriz-Bazman zone) is the main host of many Iranian porphyry and epithermal Cu, Au, and Mo mineralization deposits [26-27]. This zone is about 50 to 100 km thick and mostly consists of an Andean-type magmatic arc adjoining the Central Iranian Micro-Continent (CIMC). In the structural geologic division map of Iran, the UDMA is characterized by the Cenozoic magmatic rocks of the Eocene-Quaternary age and their associated volcanoclastic rocks. Magmatic intrusions are mostly dominated by subvolcanic porphyritic granitoid units of granite, granodiorite, diorite, and tonalite [28-29]. Fig. 1 illustrates the structural geologic map of Iran, on which the UDMA elongates from the NW to SE of the country. The Agh-Daragh area is located in the northwestern portion of the belt.

The simplified geological setting of the area is presented in Figs. 2 and 3a. In the western portions of the area and in the north of the granodiorite masses, there is a sequence of green tuffs and volcanic ashes related to the Cretaceous period. In the NE of the Gavdel village, there is a sedimentary unit, whose general color is dark gray and is generally composed of shale and limestone units. The main plutonic suite in the region, which is related to the Shiverdagh plutonic mass, is a porphyry granodiorite unit with pink feldspar phenocrysts [32].

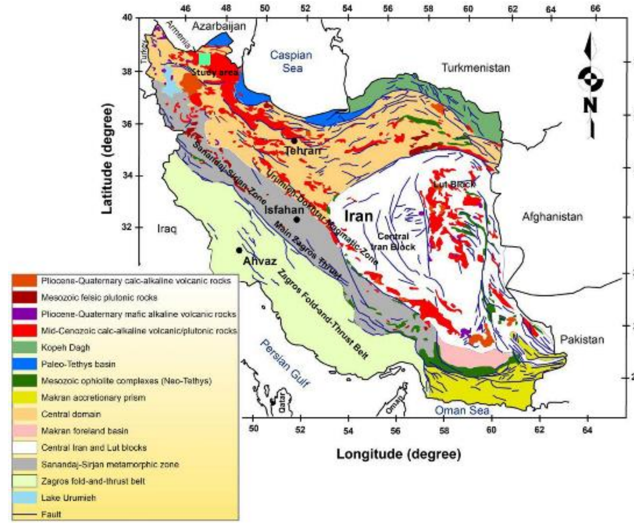

Fig. 1. Structural geologic map of Iran, on which the location of the study area is presented in the NW portion, over the UDMA zone (modified after Richards et al. 2006) [30].

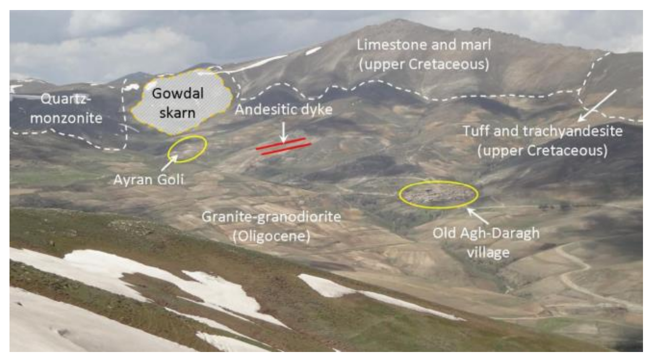

Fig. 2. Field photo of different lithological units in the Agh-Daragh prospect zone, on which the location of the Ghalandar Cu mineralization (comprising the Ayran Goli and Gowdal mineralization systems) has been portrayed (Asgharzadeh Asl et al. 2017) [31].

The Ghalandar deposit (comprising the Ayran Goli and Gowdal skarn deposits) is located about 23 km north of Ahar, Eastern Azerbaijan province, NW Iran. Previous studies have stated the presence of Cu-Fe mineralization potentials in this area, in which the main mineral deposits are of porphyry and skarn systems. The porphyry systems dominate the SE regions, while the skarn systems are located in the western regions [33-34]. Fig. 3a shows the geologic map of the Agh-Daragh prospect zone and Fig. 3b presents the detailed geological setting of the Ghalandar Cu-Fe porphyry-skarn deposit.

3. Geophysical Electrical Survey

Considering the nature of Cu mineralization in the Ghalandar region, the ERT survey was carried out to delineate sulfide-related minerals. Scintrex IPR 12 equipment was used for data acquisition. Seven 2D ERT profiles with S-N directions were designed to acquire the information about the electrical resistivity and induced polarization properties of subsurface materials. An electrode spacing of 30 m with a line spacing of 100 m was conducted in the survey. The pole-dipole array was implemented based on the ERT configuration to inject the DC current into deeper locations. The layout of the ERT survey is indicated in Fig. 3b, showing that sixteen boreholes were drilled based on geophysical data modeling used to construct the geometry of sulfide-bearing Cu mineralization. The overall length of the drilling was about 2760 m. Fig.

4 presents a 3D visualization of all drilling with respect to the topographic surface, along with Cu grades.

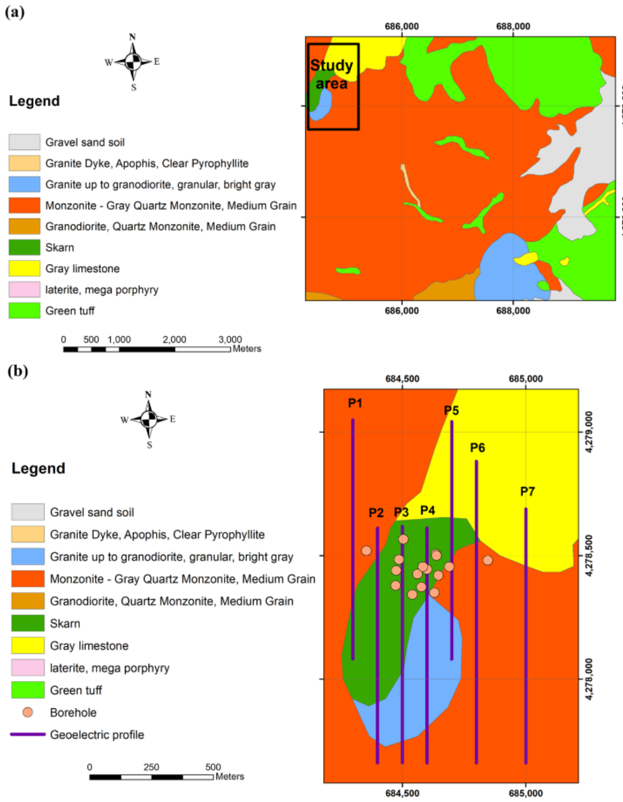

Fig. 3. Geologic map of the Agh-Daragh prospect zone (scale 1:25,000) (a), and the detailed geological setting of the Ghalandar Cu-Fe porphyry-skarn deposit (b).

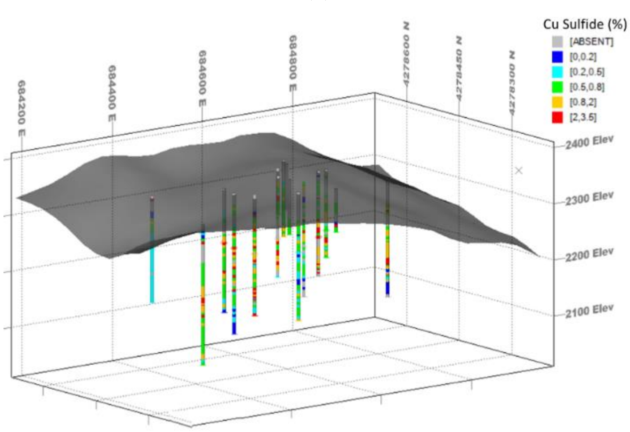

Fig. 4. Location of boreholes with respect to the topographic surface in the study area. Cu grades are shown along each borehole as well.

The 2D inversion of the ERT data was carried out by utilizing the Res2dinv software developed by Loke, and the inverted sections for the electrical resistivity and induced polarization are visualized in Fig. 5. The size of geo-electric pseudo-section meshes was produced on the basis of the distribution of the data points as a rough guide. The height of the bottom row of the meshes is set to be equal to the equivalent height of investigating the data points with the maximum electrode spacing.

Inversion methods aim to determine the value of blocks that will produce an apparent resistivity pseudo-section that agrees with true measurements. The height of the first layer of the meshes for the pole-dipole array was set at 0.6 times that of the electrode spacing. The height of each subsequent layer was gradually increased by 10% [35]. The length of the blocks was equal to the electrode spacing in this study. The inverted models were such that the predicted data had the lowest misfit with original observations. Profile 4 was chosen as the representative of all ERT profiles to show the close consistency of drilled borehole neighboring the inverted section shown in Fig 6. The electrical models in profile 4 were estimated to the nearest borehole through the nearest neighborhood method to be able to compare them with Cu grades. Subsequently, the cross-correlation plots between Cu-Rs and Cu-IP were prepared, as displayed in Fig. 7. Pearson's linear correlation coefficients between Cu and the electric variables were obtained to be equal to -0.76 and +0.81 for Rs and IP models, respectively. It should be mentioned that the higher values of Cu grades corresponded to lower and higher values of resistivity and induced polarization, respectively.

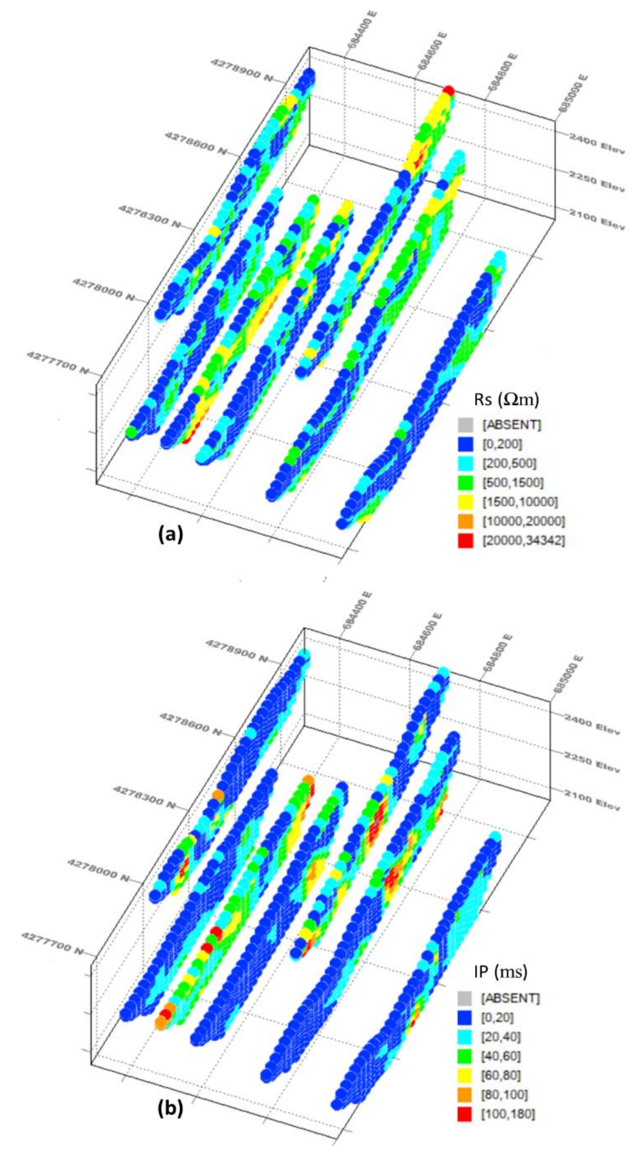

Fig. 5. 3D visualization of all 2D inverted profiles of electrical resistivity (a), and chargeability (b).

Since Cu enrichment was correlated with anomalous electrical models, constructing the 3D models of physical properties could provide insights into the geometry of the Cu mineralization in the Ghalandar region. Therefore, the following section discusses how geostatistical-based approach can facilitate the 3D recovering of electrical models from interpolating 2D inverted results shown in Fig. 5.

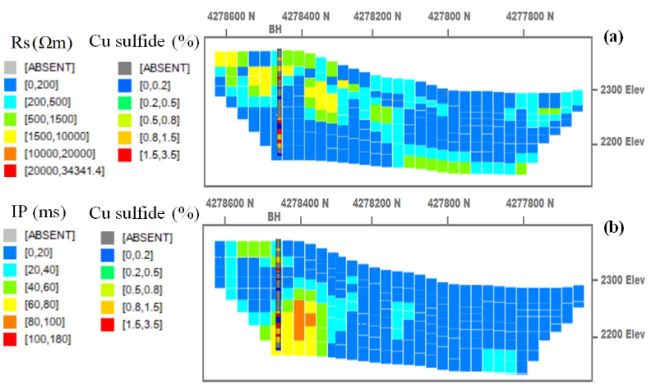

Fig. 6. A cross-section view of the 2D inverted models of the electrical resistivity (a), and the induced polarization (b) along profile 4, on which Cu grades along the drilled borehole next to the ERT survey are overlain on the sections.

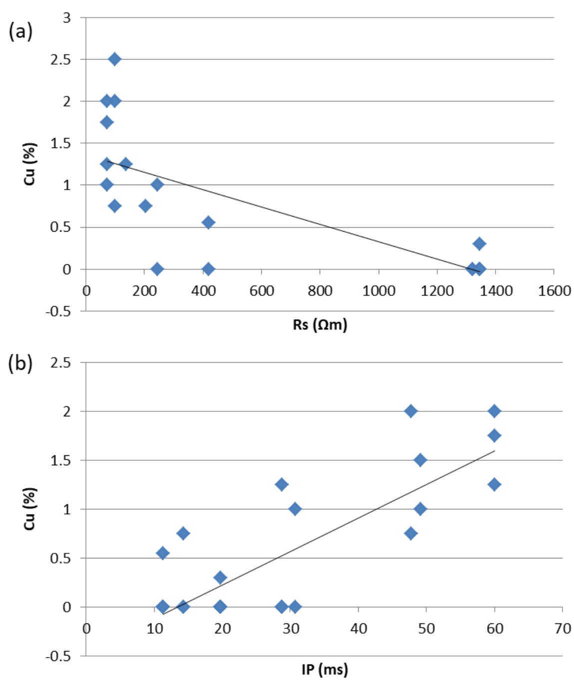

Fig. 7. Scatter plots of Cu grades along the borehole near the ERT survey versus the electrical resistivity (a) and chargeability (b) for profile 4.

4. Geostatistical Models

This section discusses the procedure of constructing 3D models of two electrical properties along with the block model of Cu grades derived from exploratory boreholes. All boreholes in this study were drilled vertically. According to the distance between the boreholes, the block model dimensions were 20×20×10 m^3wa to generate the three aforementioned models. The statistical descriptions of the variables (i.e. Rs, IP, and Cu grade) derived from their composited models are summarized in Table 1. The histogram and box-plot of these variables are shown in Fig. 8, indicating a skewed distribution of each variable.

Since a spatial structure is important for implementing any geostatistical method, a variogram model is required to be determined in multiple directions. This tool can provide the main parameters for kriging estimations. Therefore, the accuracy of calculated variogram parameters has a substantial effect on the interpolated variable [36]. The directional variogram models for three variables were searched, and the highest spatial continuity for electrical resistivity, induced polarization, and Cu grade are shown in Fig. 9. Table 2 lists the main parameters of each videography, assuming a spherical model fitted to each variable.

Table 1. Aa summary of statistical properties of the variables: Rs, IP, and Cu grade.

	Number	Mean	Variance	Maximum
Rs	606	755.98	2.17E+06	16676.1
IP	606	37.52	1310.46	172.85
Cu Sulfide	378	0.75	0.39	3.5
	Upper quartile	**Median**	**Lower quartile**	**Minimum**
Rs	706.77	351.14	153.88	4.05
IP	49.12	26.66	12.23	0.04
Cu Sulfide	1	0.5	0.5	0

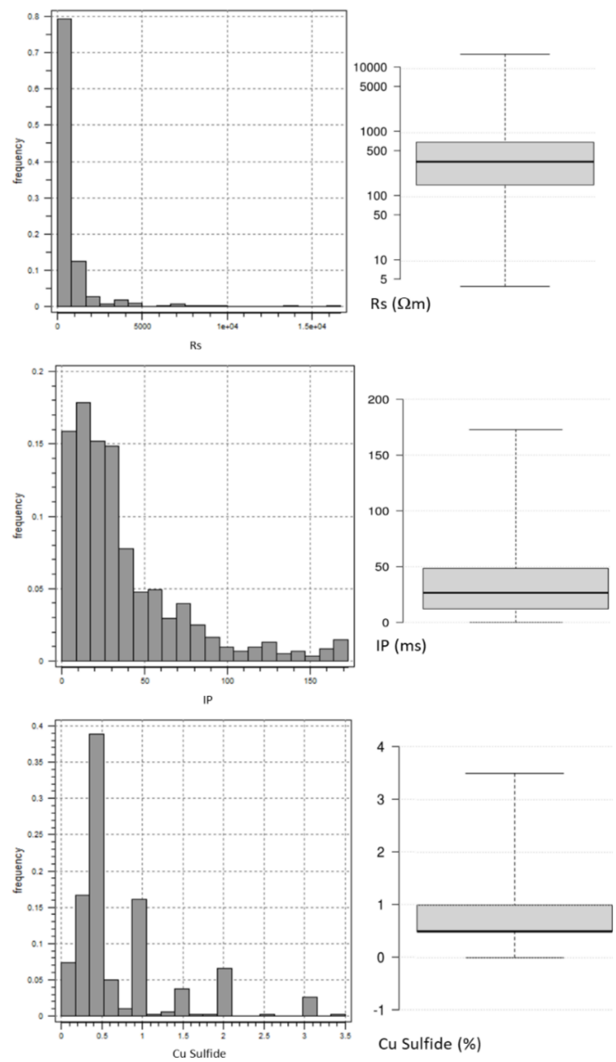

Fig. 8. The histogram and box-plot for the electrical resistivity (1st row), chargeability (2nd row), and Cu Sulfide content (3rd row).

In order to evaluate the accuracy of searched variogram models, a cross-validation method was taken into account to re-estimate the left-out data. Indeed, this validation method examines that the left-out data, and therefore, the desired statistical parameters must be reproduced by the estimated model. The comparison between the estimated and actual values shows the accuracy of the interpolation technique [37]. Here, a 2D cross-section of electrical properties and one borehole were left to be re-estimated by the aforementioned variogram model using the kriging method. The scatter plots of estimated versus original ones were presented in Fig. 10. Pearson's linear correlation coefficients between actual and estimated values were obtained equal to 0.86, 0.92, and 0.77 for electrical resistivity, chargeability, and Cu grade, respectively. These values state that the variogram parameters provide sufficient accuracy for 3D modeling.

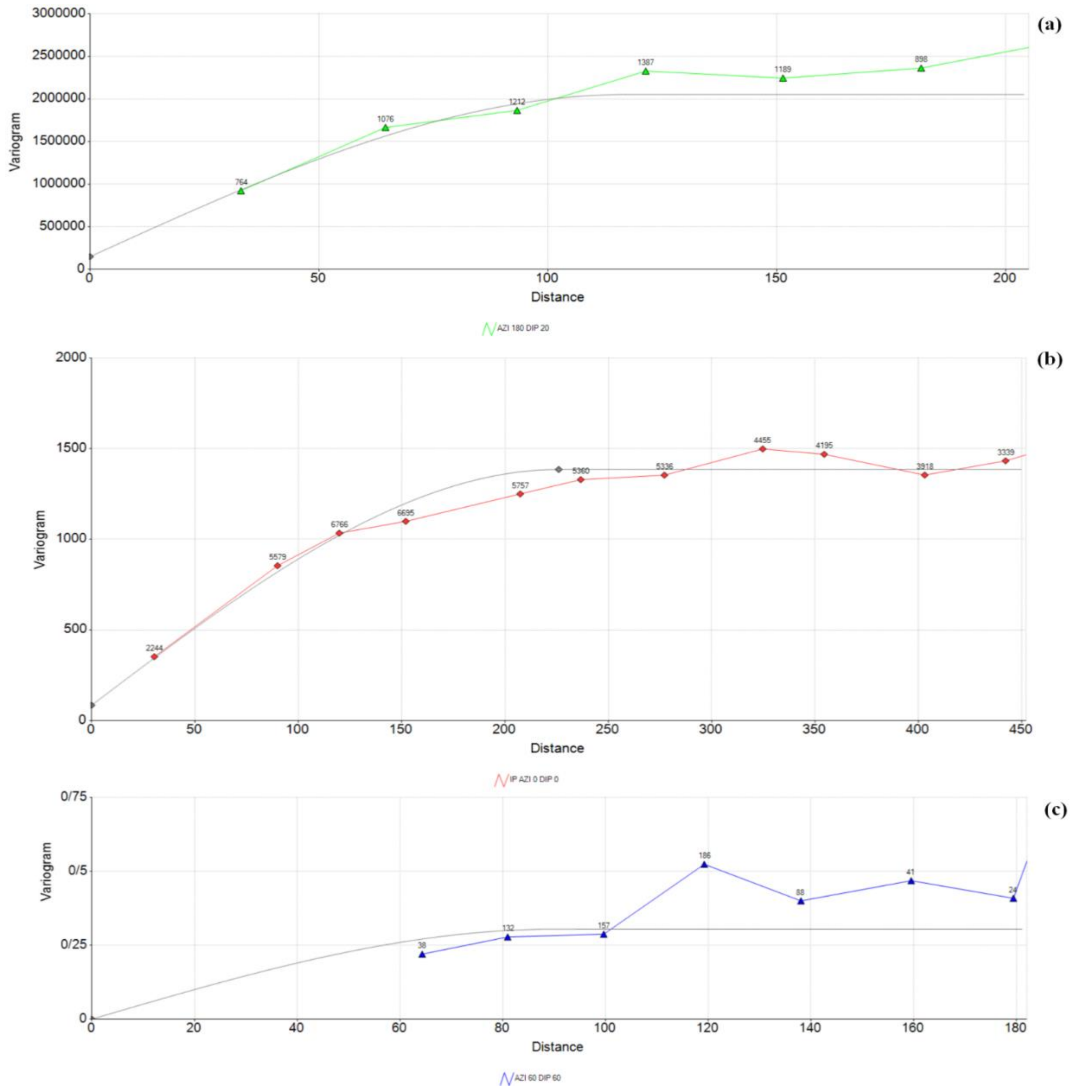

Fig. 9. Experimental directional semi-variogram models, and the number of pairs for (a) the electrical resistivity, (b) induced polarization, and (c) Cu grade.

Table 2. Variogram model parameters obtained for the three variables.

	Azimuth	Dip	Range	Sill	Nugget	Model
IP	0	0	225	1300	20	spherical
Rs	180	20	117	2100000	148706	spherical
Cu Sulfide	60	60	90	0.3	0	spherical

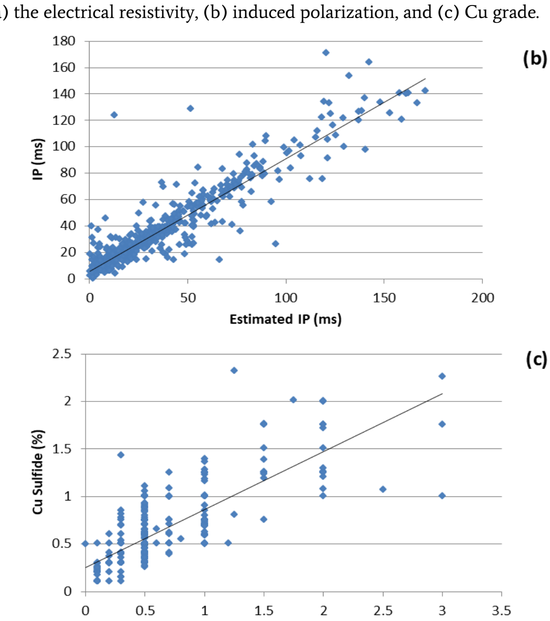

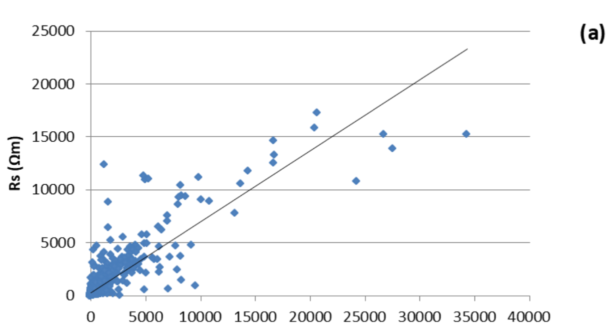

Fig. 10. Scatter plots of actual and estimated values for electrical resistivity (a), chargeability (b), and Cu sulfide content (c).

After determining the required inputs for implementing kriging, the 3D models of Cu grade, IP, and Rs were interpolated as well. The anomalous zones for each variable in the 3D model are visualized in Fig. 11. Also, the threshold values are determined by a multi-fractal analysis to plot the models. Discussing the procedure of implementing a fractal-based method is beyond the aims of this study.

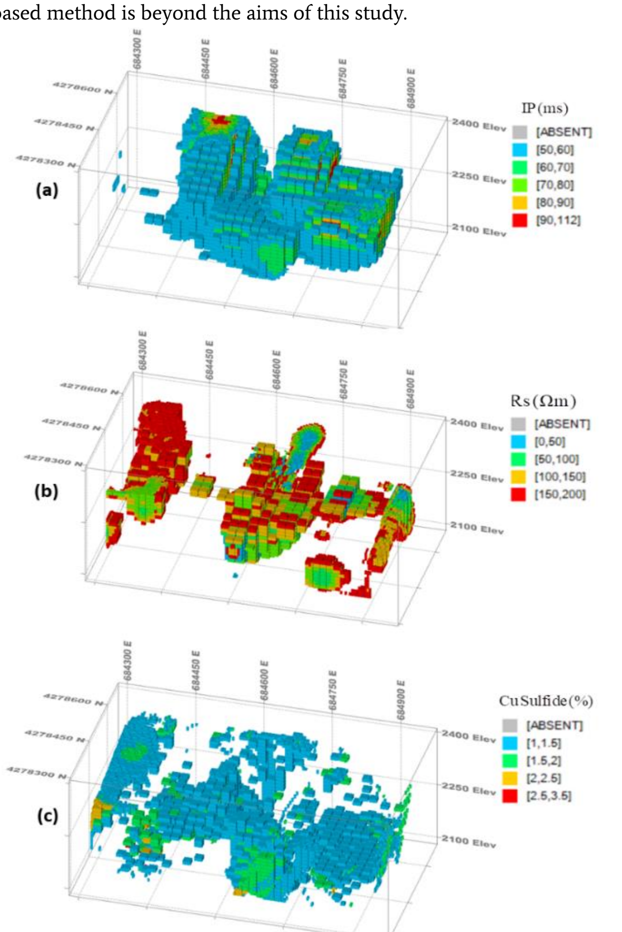

Fig. 11. 3D models of induced polarization (a), resistivity (b), and Cu Sulfide content (c) in the study area. Threshold values were assumed equal to 50-112 ms, less than 200 Ohm.m, and higher than 1.1 %, respectively.

It should be noted that the 3D model of Cu mineralization acquired from the electrical properties has a distinct E-W strike. Such a meaningful correlation can localize the probable anomalous zones of mineralization for further exploratory drilling to determine its mineral prospectivity in the area of interest.

An evaluation matrix was used to validate the results. The evaluation matrix presents the overall accuracy by an amount derived from the ratio of the total correct results over the total number of data. By dividing the trace of the matrix by the total number of data laying at an interval of 0-1, the results of 3D modeling were compared to each other. For instance, the number of anomalous IP blocks in the copper mineralization zone was 4447, and the number of anomalous IP out of the copper mineralization zone was 2414. Simultaneously, the number of non-anomalous IP blocks in the copper mineralization zone was 11720, and the number of non-anomalous blocks out of the copper mineralization was 15165. It yielded an accuracy of 0.58 extracted from the evaluation matrix shown in Table 3. This index was also calculated between Rs and Cu models in Table 4, showing an accuracy of 0.54.

Table 3. Evaluation matrix of IP and Cu grade estimations to test the performance of the 3D models.

Cu mineralization Zone	Anomalous IP block	Non-anomalous IP block
Inside	4447	11720
Outside	2414	15165

In order to optimize the results and reduce the error, the IP and Rs anomalous zones were extracted simultaneously (Fig. 12), where both electrical models approve the probable location of Cu mineralization. In this case, the overall accuracy of the evaluation matrix increased to 0.6. The results show that the integration of IP and Rs has a better result for imaging Cu mineralization in comparison with their individual models. The integrated evaluation matrix is shown in Table 5.

Table 4. Evaluation matrix of Rs and Cu estimations to test the performance of the 3D models.

Cu mineralization Zone	Anomalous Rs block	Non-anomalous Rs block
Inside	3414	12749
Outside	2724	14850

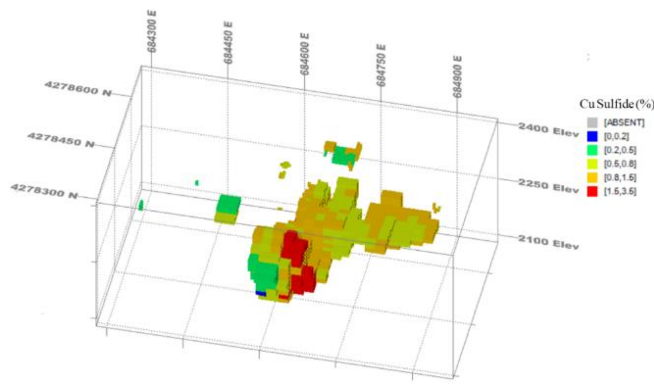

Fig. 12. The 3D model of Cu grade made from the integration of IP and Rs anomalous zones.

Table 5. Evaluation matrix of integrated IP-Rs and Cu grade estimations to evaluate the performance of 3D models.

Cu mineralization Zone	Anomalous Rs and IP block	Non-anomalous Rs and IPblock
Inside	870	9175
Outside	229	12670

Another comparison approach is the swath plot, which is a graphical representation of a variable distribution from a series of slices assumed in three main directions of the block model [38]. For this purpose, the block model was divided into several slices in three main directions (NS, EW, and down-hole directions) and the average of block estimates (Cu, Rs, and IP) falling inside each slice was calculated. Finally, the average values were plotted against the corresponding direction (Fig. 13). It should be mentioned that the borehole and geophysical variables were normalized between -1 and 1 in order to compare the results better.

All plots were derived from block models shown in Fig. 12, which means all swath plots are related to the anomalous zone. As a general trend, the values of IP and Cu have a reverse trend in comparison with the Rs value, and they all fluctuate along the X-axis. IP and Cu values show a decreasing trend along the Y-axis, while Rs values show an increasing trend along the Y-axis. The trends along the Z-axis are almost the same as the Y-axis.

5. Conclusion

The performance of 3D electrical models was discussed for the Agh-Daragh porphyry-skarn copper deposit located in the Eastern Azerbaijan province of Iran. A geostatistical-based approach was utilized to interpolate the 3D geophysical models of electrical resistivity and induced polarization derived from the 2D inversion. The results of the kriging technique conducted on physical properties were in close association with the Cu model constructed from 16 boreholes in the Ghalandar prospect zone. Such correlation was confirmed by calculating the evaluation matrix between geophysical models and the Cu mineralization. The interesting result was obtained when the integrated geophysical model had a higher correlation with the mineralized zones. The swath plots were carried out as the second validation method showing a high correlation between the anomalous zones.

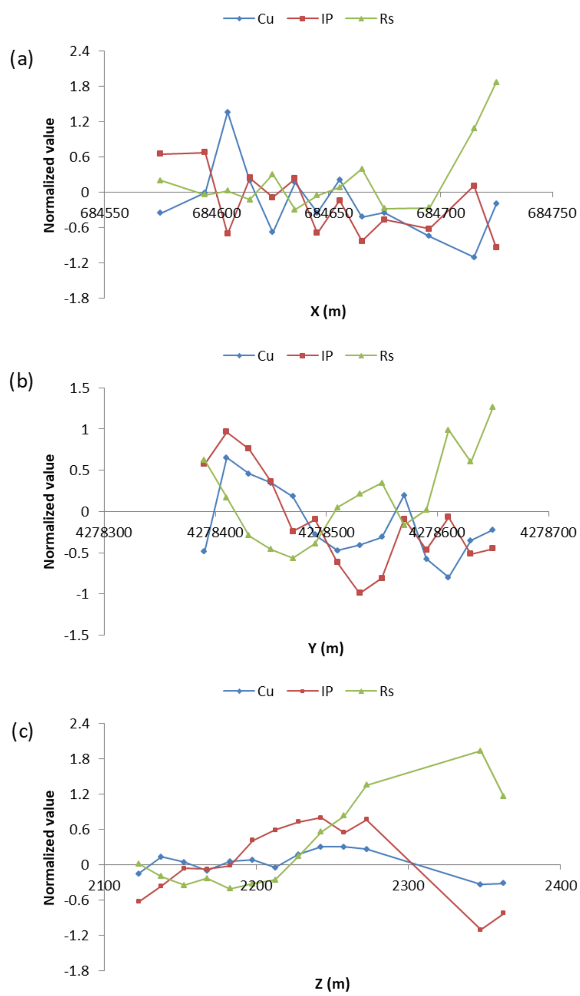

Fig. 13. Normalized Swath plots of Cu, IP, and Rs values in the direction E-W (a), N-S (b), and vertical (c).

Acknowledgments

The authors express their sincere gratitude to the School of Mining Engineering, University of Tehran, for all technical and financial supports.

REFERENCES

[1] Sun, J., & Li, Y. (2014). Exploration of a sulfide deposit using joint inversion of magnetic and induced polarization data. In SEG Technical Program Expanded Abstracts 2014 (pp. 1780-1784). Society of Exploration Geophysicists.

[2] Telford, W. M., Geldart, L. P., Sheriff, R. E. (1990). Applied geophysics (Vol. 1). Cambridge university press.

[3] Oldenburg, D. W., Li, Y., & Ellis, R. G. (1997). Inversion of geophysical data over a copper gold porphyry deposit: a case history for Mt. Milligan. Geophysics, 62(5), 1419-1431.

[4] Mostafaei, K., & Ramazi, H. R. (2018). 3D model construction of induced polarization and resistivity data with quantifying uncertainties using geostatistical methods and drilling (Case study: Madan Bozorg, Iran). Journal of Mining and Environment, 9(4), 857-872.

[5] Irvine, R. J., & Smith, M. J. (1990). Geophysical exploration for epithermal gold deposits. Journal of Geochemical exploration, 36(1-3), 375-412.

[6] Allis, R. G. (1990). Geophysical anomalies over epithermal systems. Journal of Geochemical Exploration, 36(1-3), 339-374.

[7] Bakkali, S. (2006). A resistivity survey of phosphate deposits containing hardpan pockets in Oulad Abdoun, Morocco. Geofísica internacional, 45(1), 73-82.

[8] Locke, C. A., Johnson, S. A., Cassidy, J., & Mauk, J. L. (1999). Geophysical exploration of the Puhipuhi epithermal area, Northland, New Zealand. Journal of Geochemical Exploration, 65(2), 91-109.

[9] Moreira, C. A., Rezende Borges, M., Vieira, L., Matheus, G., Malagutti Filho, W., & Fernándes Montanheiro, M. A. (2014). Geological and geophysical data integration for delimitation of mineralized areas in a supergene manganese deposits. Geofísica internacional, 53(2), 199-210.

[10] Vieira, L. B., Moreira, C. A., Côrtes, A. R., & Luvizotto, G. L. (2016). Geophysical modeling of the manganese deposit for Induced Polarization method in Itapira (Brazil). Geofísica internacional, 55(2), 107-117.

[11] Pelton, W. H., Ward, S. H., Hallof, P. G., Sill, W. R., & Nelson, P. H. (1978). Mineral discrimination and removal of inductive coupling with multifrequency IP. Geophysics, 43(3), 588-609.

[12] Vanhala, H., & Peltoniemi, M. (1992). Spectral IP studies of Finnish ore prospects. Geophysics, 57(12), 1545-1555.

[13] Thoman, M. W., Zonge, K. L., & Liu, D. (1998). Geophysical case history of North Silver Bell, Pima County, Arizona—a supergene-enriched porphyry copper deposit. Northwest Mining Association, 42.

[14] John, D. A., Ayuso, R. A., Barton, M. D., Blakely, R. J., Bodnar, R. J., Dilles, J. H., ... & Seal, R. R. (2010). Porphyry copper deposit model, chap. B of Mineral deposit models for resource assessment. US Geological Survey Scientific Investigations Report, 2010, 1-169.

[15] Sinclair, W. D. (2007). Porphyry deposits. Mineral deposits of Canada: A synthesis of major deposit-types, district metallogeny, the evolution of geological provinces, and exploration methods: Geological Association of Canada, Mineral Deposits Division, Special Publication, 5, 223-243.

[16] Brant, A. A. (1966). Geophysics in the exploration for Arizona porphyry coppers. Geology of the porphyry copper deposits: southwestern North America. University of Arizona Press, Tucson, 87-110.

[17] Niederleithinger, E. (2015). 3G-Geophysical Methods Delivering Input to Geostatistical Methods for Geotechnical Site Characterization.

[18] Tang, H. (2005). Geostatistical integration of geophysical well bore and outcrop data for flow modeling of a deltaic reservoir analogue.

[19] Pendrel, J. V. (2013). Integrating geologic and geophysical data in geostatistical inversion: GeoConvention 2013: Integration.

[20] Bourges, M., Mari, J. L., & Jeannée, N. (2012). A practical review of geostatistical processing applied to geophysical data: methods and applications. Geophysical Prospecting, 60(3), 400-412.

[21] Ramazi, H., & Jalali, M. (2015). The contribution of geophysical inversion theory and geostatistical simulation to determine geoelectrical anomalies. Studia Geophysica et Geodaetica, 59(1), 97-112.

[22] Asghari, O., Sheikhmohammadi, S., Abedi, M., & Norouzi, G. H. (2016). Multivariate geostatistics based on a model of geo-electrical properties for copper grade estimation: a case study in Seridune, Iran. Bollettino di Geofisica Teorica ed Applicata, 57(1).

[23] Berberian, F., & Berberian, M. (1981). Tectono-plutonic episodes in Iran. Zagros Hindu Kush Himalaya Geodynamic Evolution, 3, 5-32.

[24] StScklin, J. (1968). Structural history and tectonics of Iran. AAPG Bull, 52(7), 1229-58.

[25] Nouri, F., Azizi, H., Stern, R. J., Asahara, Y., Khodaparast, S., Madanipour, S., & Yamamoto, K. (2018). Zircon U-Pb dating, geochemistry, and evolution of the Late Eocene Saveh magmatic complex, central Iran: Partial melts of sub-continental lithospheric mantle and magmatic differentiation. Lithos, 314, 274-292.

[26] Berberian, M., & King, G. C. P. (1981). Towards a paleogeography and tectonic evolution of Iran. Canadian journal of earth sciences, 18(2), 210-265.

[27] Rezaei, S., Lotfi, M., Afzal, P., Jafari, M. R., Meigoony, M. S., & Khalajmasoumi, M. (2015). Investigation of copper and gold prospects using index overlay integration method and multifractal modeling in Saveh 1: 100,000 sheet, Central Iran. Gospodarka Surowcami Mineralnymi, 31(4), 51-74.

[28] Shahabpour, J. (2005). Tectonic evolution of the orogenic belt in the region located between Kerman and Neyriz. Journal of Asian Earth Sciences, 24(4), 405-417.

[29] Kazemi, K., Kananian, A., Xiao, Y., & Sarjoughian, F. (2018). Petrogenesis of Middle-Eocene granitoids and their Mafic microgranular enclaves in central Urmia-Dokhtar Magmatic Arc (Iran): Evidence for interaction between felsic and mafic magmas. Geoscience Frontiers.

[30] Richards, J. P., Wilkinson, D., & Ullrich, T. (2006). Geology of the Sari Gunay epithermal gold deposit, northwest Iran. Economic Geology, 101(8), 1455-1496.

[31] Asl, H. A., Mehrabi, B., & Fazel, E. T. (2017). Mineralogy, occurrence of mineralization and temperature-pressure conditions of the Agh-Daragh polymetallic deposit in the Ahar-Arasbaran metallogenic area. Journal of Economic Geology, 9(9), 1-23.

[32] Mehrabi, E., Masoudi, F., Jamali, H., Asgharzadeh, H. (2013). Petrography, alteration, and mineralization of Agh-Daragh region. 17th Conference of Iranian Geological Society. Tehran, Iran. (Published in Persian).

[33] Kazem Alilou, S. (2015). Application of Fuzzy decision making approach in 2D mineral potential mapping and its comparison with 3D magnetic geophysical presentation in Ghalandar Zone, West Azerbaijan province of Iran. MSc. Thesis in University of Tehran, 1113 p. (Published in Persian).

[34] Kazem Alilou, S., Abedi, M., Norouzi, GH., Dowlati, F. (2013). Application of magnetometry, special resistivity and induced polarization for exploration of iron and copper skarn deposits, a case study: Ghalandar, Ahar. 1st national conference of exploration engineering, University of Shahroud (Published in Persian).

[35] Loke, M. H. (2004). Tutorial: 2-D and 3-D electrical imaging surveys.

[36] Mostafaie, K., Ramazi, H., & Jalali, M. (2014). Application of Integrated Geophysical and Geostatistical Methods in Amiriyeh Site Classification. Geodynamics Research International Bulletin (GRIB), 2(2), 1-15.

[37] Deutsch, C. V. (2010). Display of cross validation/jackknife results. Centre for Computational Geostatistics Annual Report, 12(406), 1-4.

[38] Ertunç, G., Tercan, A. E., Hindistan, M. A., Ünver, B., Ünal, S., Atalay, F., & Kıllıoğlu, S. Y. (2013). Geostatistical estimation of coal quality variables by using covariance matching constrained kriging. International Journal of Coal Geology, 112, 14-25.